# QUARK NOVA SIGNATURES IN SUPER-LUMINOUS SUPERNOVAE

M. Kostka,[1] N. Koning,[1] D. Leahy, [1] R. Ouyed,[1] and W. Steffen[2]

RESUMEN

Censos observacionales recientes han revelado la existencia de supernovas super-luminosas (SLSNe). En este trabajo estudiamos las curvas de luz de ocho SLSNe en el contexto del modelo de las novas-quark de choque dual. Encontramos que estrellas progenitoras con masas entre 25 y $35 M_\odot$ proporcionan energía más que suficiente para explicar las curvas de luz de las SLSNe. Se examinan los efectos de una variación de los parámetros físicos de la nova-quark de choque dual sobre las curvas de luz. Concluimos que la amplia variedad de morfologías de las curvas de luz de las SLSNe puede ser explicada principalmente por variaciones en el lapso de tiempo entre la supernova y la nova-quark. Nuestro análisis muestra que el perfil H$\alpha$ singular encontrado en tres SLSNe puede ser descrito naturalmente en el escenario de las novas-quark de choque dual. Se presentan algunos rasgos espectrales predichos específicamente por el modelo de las quark-novas de choque dual.

ABSTRACT

Recent observational surveys have uncovered the existence of super-luminous supernovae (SLSNe). In this work we study the light curves of eight SLSNe in the context of dual-shock quark novae. We find that progenitor stars in the range of $25 - 35 M_\odot$ provide ample energy to power each light curve. An examination into the effects of varying the physical properties of a dual-shock quark nova on light curve composition is undertaken. We conclude that the wide variety of SLSN light curve morphologies can be explained predominantly by variations in the length of time between supernova and quark nova. Our analysis shows that a singular H$\alpha$ spectral profile found in three SLSNe can be naturally described in the dual-shock quark nova scenario. Predictions of spectral signatures unique to the dual-shock quark nova are presented.

*Key Words:* dense matter — radiative transfer — stars: evolution — supernovae: general

## 1. INTRODUCTION

The standard astrophysical explanation for a supernova (SN) is that the radiated power is generated by energy deposited in expanding ejecta through one of three mechanisms: the SN shock travels through the stellar envelope (Grassberg et al. 1971), radioactive decay of heavy elements synthesized in the explosion (Arnett 1982) or a collision with hydrogen-rich circumstellar material (CSM) (Chevalier 1982). In 2011 astronomers working on the Palomar Transient Factory announced the emergence of a new class of SNe that cannot be explained by any of these means (Quimby et al. 2011). As described by Quimby et al. (2011) this new class of SNe is at least ten times brighter than a typical type Ia SN, displays spectra with little to no hydrogen, emits significant UV flux over a long period

of time and has a late stage luminosity evolution that is inconsistent with radioactive decay.

While this hydrogen-poor class of super-luminous SNe (SLSNe) is a recent admission, the phenomenon of SLSNe as a whole has been an open question since the discovery of SN 2006gy (Quimby et al. 2007b). Large scale supernovae surveys such as the Palomar Transient Factory (PTF) (Rau et al. 2009; Law et al. 2009), the ROTSE Supernova Verification Project (RSVP, formerly the Texas Supernova Search) (Quimby et al. 2005) and the Catarina Real-Time Transient Survey (Drake et al. 2009) have uncovered approximately ten other SLSNe, some of which contain hydrogen in their spectra (SN 2006gy, Quimby et al. 2007b; SN 2008fz, Drake et al. 2010) while others are hydrogen-poor (SN 2005ap, Quimby et al. 2007b; SN 2007bi, Gal-Yam et al. 2009).

One method being considered to power the radiated energy of some SLSNe is a scaled up version of a CSM interaction. A dense, massive ($\approx 20~M_\odot$) CSM

[1]Department of Physics and Astronomy, University of Calgary, Calgary, Canada.

[2]Instituto de Astronomía Universidad Nacional Autónoma de México, Ensenada, B.C., Mexico.

TABLE 1

VERY LARGE ARRAY OBSERVATIONS

| | Model | | | |
|---|---|---|---|---|
| SLSNe Property | PISN | CSM | Magnetar | dsQN |
| Energy mechanism | $\gamma = 4/3$ instability[a] | Binary merger[b] | Rotational energy[c] | QN explosion [d] |
| Radiation mechanism | Collision of ejecta[a] | CSM/SN interaction[e] | Synchrotron[c] | QN/SN interaction[d] |
| Progenitor mass ($M_\odot$) | $313^f - 1250^f$ | $100+^g$ | $8^h - 25^i$ | $20^j - 40^j$ |
| X-rays | suppressed[k] | suppressed[l] | not discussed | suppressed[j] |
| Hydrogen in spectra | unlikely[m] | necessary[n] | not discussed | likely[j] |
| Cause of long-lasting broad lines | not expected[o] | velocity of SN[g] | velocity of [p] inner shell | temperature of inner shell[j] |
| Late stage luminosity | radioactivity[a] | opaque outer region of CSM[q] | inner bubble[c] | inner shell emission[j] |

[a]Woosley et al. (2007),[b]Chevalier (2012), [c]Kasen & Bildsten (2010), [d]Leahy & Ouyed (2008), [e]Chevalier (1982), [f]Pan et al. (2012), [g]Smith et al. (2010), [h]Weidemann (1977), [i]Fryer (1999), [j]Ouyed et al. (2012), [k]Blinnikov (2008), [l]Chevalier & Irwin (2012), [m]Yungelson et al. (2008), [n]Quimby et al. (2011), [o]Kasen et al. (2011), [p]Dessart et al. (2012), [q]Chevalier & Irwin (2011).

envelope enshrouds the progenitor star at the time of the SN explosion. An efficient conversion of SN kinetic energy to radiation via the SN shock powers the SLSN light curve (Smith et al. 2008; Chevalier & Irwin 2011; Ginzburg & Balberg 2012; Kiewe et al. 2012). Building such a CSM envelope requires a mass-loss rate of $\dot{M} > 0.1\ M_\odot\ \mathrm{yr}^{-1}$ over the final 10–100 years prior to SN explosion (Moriya et al. 2013; Ginzburg & Balberg 2012). Two possible explanations for a mass-loss rate on this order are LBV-like mass ejections (Smith et al. 2008; Kiewe et al. 2012) or common envelope phase of an interacting binary system (Chevalier 2012).

An alternative description considered for SLSNe is that the radiated energy is converted from the rotational energy of a magnetar (Kasen & Bildsten 2010; Woosley 2010) inside a SN envelope. For the magnetar model to power the light curve of a SLSN, large $PdV$ losses must be avoided by delaying the conversion of the magnetar's rotational energy into radiation. An explanation for the delay in energy injection has yet to be examined. The delayed injection of energy into the SN envelope must be isotropically distributed across the inner edge of the SN envelope energizing the entire envelope and generating the radiated energy of a SLSN. Whether the magnetar model can power a SLSN with the expected jet-like (Bucciantini et al. 2009) energy deposition has yet to be studied. Dessart et al. (2012) provided an indicative study into the magnetar model explanation for the observed blue spectrum and broad spectral lines seen in most SLSNe.

Pair-instability SNe (PISNe) have as well been proposed as the underlying energy mechanism for SLSNe. In this scenario an extremely massive star becomes prone to $\gamma = 4/3$ instability, triggering a SN explosion. Pan et al. (2012) studied the progenitor stars for PISN and found that the mass range required for a star to end its life as a PISN is $\approx 300 - 1000\ M_\odot$. The predicted light curve from a PISN should be nearly symmetric (Kawabata et al. 2009; Dessart et al. 2012).

Ouyed et al. (2002) suggested that a collision between material ejected through the quark nova (QN) explosion of a neutron star and the preceding SN envelope could rebrighten the SN (see § 5.4 of Ouyed et al. 2002). This theory was first applied in the context of SLSNe by Leahy & Ouyed (2008) to explain SN 2006gy. Table 1 summarizes each proposed model's explanation for a variety of SLSNe characteristics. While acknowledging that other models are being pursued to explain SLSNe, in this work we provide the QN as a possible engine for a universal explanation for SLSNe. Observations of the SLSNe studied in this work are introduced in § 2. § 3 summarizes the explosion mechanism of the QN as well as the environment which leads to a SLSN. § 4 examines the physics implemented in describing the interaction between ejecta of a SN and a QN. Analysis of the effects of changing physical parameters on our model light curve is undertaken in § 5. In § 6 we compare observations of eight SLSNe (SN 2005ap, SN 2006gy SN 2006tf, SN 2007bi, SN 2008es, SN 2008fz, PTF09cnd and PTF10cwr to QNe of different physical parameters. A discussion of trends found fitting the SLSNe and spectral analysis for some targets is presented in § 7. Finally our conclusions as well as predicted chemical signatures of our model are discussed in § 8.

## 2. OBSERVATIONS

For this analysis we have chosen eight SLSNe (SN 2005ap, SN 2006gy, SN 2006tf, SN 2007bi, SN 2008es, SN 2008fz, PTF09cnd and PTF10cwr) to study in the context of the quark nova (Ouyed et al.

TABLE 2

LIST OF SLSNE TARGETS.

| Name | Type | Peak Magnitude | Proposed Models |
|------|------|----------------|-----------------|
| SN 2005ap | H-poor SLSN[a] | $-22.7$[b] | CSM[a], PISN[a],dsQN[c] |
| SN 2006gy | IIn[d] | $-22$ [e] | PISN[f], CSM[e], dsQN[c,g] |
| SN 2006tf | IIn[h] | $\approx -20.8$[h] | CSM[h] |
| SN 2007bi | Ic[i] | $-21.3$[i] | CC[j], PISN[i] |
| SN 2008es | II-L[k] | $-22.2$[k] | CSM[k] |
| SN 2008fz | IIn[l] | $-22.3$[l] | none[l] |
| PTF09cnd | H-poor SLSN[a] | $-22$[a] | CSM[a], PISN[a] |
| PTF10cwr | H-poor SLSN[a] | $-21.2$[m] | CSM[a], PISN[a] |

[a]Quimby et al. (2011), [b]Quimby et al. (2007b), [c]Leahy & Ouyed (2008), [d]Quimby et al. (2005), [e]Smith & McCray (2007), [f]Woosley et al. (2007), [g]Ouyed et al. (2012), [h]Smith et al. (2008), [i]Gal-Yam et al. (2009), [j]Young et al. (2010), [k]Gezari et al. (2009), [l]Drake et al. (2010), [m]Pastorello et al. (2010).

2002). Each SLSN target along with the peak magnitude, class and proposed models are summarized in Table 2.

The first SLSN ever observed was SN 2006gy (Quimby et al. 2007b) which peaked in absolute $R$ band magnitude at approximately $-22$. The spectrum of SN 2006gy is dominated by a broad H$\alpha$ emission line (Smith et al. 2010) and while SN 2006gy was exceptionally bright in visible light the event was surprisingly quiet in X-rays (Smith & McCray 2007).

Spurred by the discovery of SN 2006gy, Quimby et al. (2007b) found another extremely bright ($-22.7$ peak absolute $R$-band magnitude) SN 2005ap; which remains the brightest SLSN ever observed. The spectrum of SN 2005ap shows broad spectral lines (H$\alpha$, CIII, NIII) and similarly to SN 2006gy, SN 2005ap was quiet in X-rays (Quimby et al. 2007b).

SN 2006tf was discovered by Quimby et al. (2007a) who noted that the spectrum closely resembles that of SN 2006gy. Observations of the light curve of SN 2006tf missed the leading edge of the SLSN and thus the actual peak magnitude is unclear; however, the total radiated energy of the SLSN was at least $7 \times 10^{50}$ ergs (Smith et al. 2008). Smith et al. (2007) noted that the light curve of SN 2006tf is characterized by a very slow luminosity decay rate ($\approx 0.01$ mag day$^{-1}$). The spectra of SN 2006tf display a strong H$\alpha$ emission line that remains broad over time (Smith et al. 2008). H$\alpha$ and H$\beta$ show an interesting evolution in which the red-side of the profile remains constants while the blue-side emission wing becomes more prominent with time (Smith et al. 2008). There exists a blue-side absorption feature seen in HeI $\lambda 5876$ and OI $\lambda 7774$ that is of comparable width to the blue-side absorption feature of H$\alpha$ (Smith et al. 2008).

Gal-Yam et al. (2009) discovered the SLSN SN 2007bi and identified it as a type Ic SN, noting that there was no sign of a CSM interaction. The light curve of SN 2007bi peaks at $\approx -21.3$ in the $R$ band and displays a slow luminosity decay rate ($\approx 0.01$ mag day$^{-1}$) (Gal-Yam et al. 2009). As discussed by Young et al. (2010), the relatively high host galaxy metalicity is inconsistent with a PISN explanation for the SLSN. The slowly evolving spectra of SN 2007bi show strong oxygen and iron lines (Young et al. 2010).

Discovered by Gezari et al. (2009), the light curve of SN 2008es peaks at $\approx -22.2$ in the $R$ band and shows a fast luminosity decay rate ($\approx 0.042$ mag day$^{-1}$). The total radiated energy in UV and visible is in excess of $10^{51}$ ergs; however, consistent with other SLSN, SN 2008es was quiet in X-rays (Gezari et al. 2009). The spectrum of SN 2008es is dominated by broad features that lack the narrow and intermediate width line emission typically associated with a CSM interaction (Miller et al. 2009). The spectral evolution of SN 2008es shows that the broad components of the spectral lines become more prominent over time (Miller et al. 2009).

SN 2008fz was discovered by Drake et al. (2010) who found the light curve to peak at $\approx -22.3$ in the $V$ band and to show a similar slow evolution to that of SN 2006gy. The spectrum of SN 2008fz displays strong Balmer lines that are initially narrow but become broad over time, Drake et al. (2010) noted that the H$\alpha$ emission line of SN 2008fz is similar to that of SN 2006gy for the same epoch.

We chose to study PTF09cnd and PTF10cwr as representative members of the new hydrogen-poor SLSN class (Quimby et al. 2011). These SLSNe were selected because they display the two extremes of light curve morphology for this class, PTF09cnd has the brightest and broadest $u$-band light curve in the class and PTF10cwr the dimmest and narrowest.

The luminosity decay rate of both PTF09cnd and PTF10cwr are inconsistent with radioactive decay and the spectrum shows no signs of a CSM interaction

(Quimby et al. 2011). PTF10cwr was also observed in the $B$ band by Pastorello et al. (2010), in which it peaks at $\approx -21.2$, and alternatively is referred to as SN 2010gx. As mentioned in the supplemental material associated with Quimby et al. (2011), the SLSNe PTF09cnd and PTF10cwr are quiet in X-rays relative to the amount of energy radiated in the visual bands.

## 3. QUARK NOVA

The idea that nuclei could collapse into quark matter and the possible existence of quark stars have been theorized for several decades (Itoh 1970; Bodmer 1971). Witten (1984) conjectured that up-down-strange (UDS) quark matter is a state of matter more stable than $^{56}Fe$. Within the hypothesis that UDS matter is the true ground state of hadrons the proposition that a neutron star could convert to a UDS quark star (further to be referred to simply as a quark star) was put forth by Alcock et al. (1986). They detailed numerous possible mechanisms for achieving the requisite strangeness to convert a neutron star into a quark star. Different astrophysical scenarios which could achieve this phase transition have been proposed. One such possibility is during or shortly after a SN, when the core density of the proto-neutron star is high enough to trigger quark deconfinement (Dai et al. 1995; Xu et al. 2001). Another candidate involves converting a neutron star to a quark star (Olinto 1987; Cheng & Dai 1996; Bombaci & Datta 2000). The scenario in which the quark matter core contracts in such a way that a physical separation between the core and the overlaying neutron star material develops was proposed by Ouyed et al. (2002), who introduced the concept of the QN.

### 3.1. *Explosive Mechanism*

The QN converts gravitational energy and nuclear binding energy into internal energy (heat) and partially into kinetic energy, with the majority of the energy transported via neutrinos. Investigations of neutrino and photon emission from a QN found that $10^{-5} - 10^{-3} M_\odot$ could be ejected with up to $10^{53}$ erg of kinetic energy, which means ejecta with a Lorentz factor of 10–100 (Vogt et al. 2004; Ouyed et al. 2009). Detailed studies of hadronic to UDS burning suggested that turbulence in the conversion front enhances the burning speed to sonic or supersonic velocities, which in turn would make the transition from neutron star to quark star detonative and provide another potential mechanism for mass ejection (Niebergal et al. 2010; Ouyed et al. 2011b).

### 3.2. *Timing*

The time scale for the conversion of the hadronic neutron star to a quark star is dependent on the central pressure of the neutron star and its gravitational mass

(Berezhiani et al. 2003). It has been shown that for massive neutron stars either the accretion of SN fall-back material or the spin-down evolution can cause the core density to exceed that of quark deconfinement, triggering a QN (Staff et al. 2006).

The length of time between the SN and QN explosion ($t_{delay}$), effectively the time it takes for the central density of the neutron star to exceed quark deconfinement, can vary from seconds to years (Berezhiani et al. 2003; Staff et al. 2006). This time delay plays a crucial role in determining the subsequent evolution of the stellar remnant. When the delay is short ($\lesssim 8$ days) the SN envelope is still dense and the energy of the impacting QN ejecta is used up spallating the inner region of the SN envelope (Ouyed et al. 2011a). This leads to the destruction of $^{56}Ni$ and the formation of $^{44}Ti$ and results in a subluminous SN. The reduced luminosity is due to the lack of radioactive decay of $^{56}Ni$ (Ouyed et al. 2011a). When the time delay is long (of the order of months or longer) the SN envelope will have become too diffuse to significantly interact with the QN ejecta. For massive QN ejecta with long time delays fall-back of the ejected material can occur which has implications for $\gamma$-ray bursts, soft $\gamma$-ray repeaters and anomalous X-ray pulsars (Ouyed et al. 2007a,b; Koning et al. 2012).

This work will focus on the scenario in which a SN is followed on the order of weeks by a QN. In this case, referred to as a dual-shock QN (dsQN), the expanded SN envelope is bombarded by the QN ejecta reheating the SN envelope. The extended size and high temperature of the re-shocked SN envelope yields a brilliant radiance capable of reproducing the observed luminous peaks of SLSNe. As the radiation from the extended envelope fades, an inner region of mixed QN and SN material is revealed which can explain both the luminosity decay rate of SLSNe as well as curious spectral features.

## 4. DUAL-SHOCK QUARK NOVA

The evolution of a dsQN can be considered as three distinct phases; *delay, shock* and *cooling*. During the *delay* phase the SN envelope expands homologously ($v \propto r$) while the neutron star evolves towards a QN explosion. For fiducial values the radius of the SN envelope will reach $\approx 10^{15}$ cm during this phase. The end of the *delay phase* is marked by the detonation of the QN.

At the beginning of the *shock* phase the ultra-relativistic QN ejecta (Keränen et al. 2005; Ouyed & Leahy 2009) quickly catch up and slam into the inner edge of the SN envelope. This collision creates a shock front that propels through the SN envelope reheating it to a temperature $\approx 10^9$ K (Leahy & Ouyed 2008). As the shock progresses, the inner region of the re-shocked SN envelope mixes with the impacting

QN ejecta to create a thin shell interior to the envelope, referred to as the hot plate in Ouyed et al. (2012) (hereinafter Paper I).

The end of the *shock* phase and beginning of the *cooling* phase is defined to be the moment when the shock breaks out of the SN envelope. By this time the inner shell will be fully formed and slowly coasting inside of the shocked envelope. During the *cooling* phase both the envelope and the inner shell will cool via adiabatic expansion and radiative emission. Following the same methodology used in Paper I, for the work presented here we model the light curves of dsQNe during their *cooling* phase.

### 4.1. *The Inner Shell*

As the QN ejecta ploughs through the SN envelope material builds up to form the inner shell. The mass $(M_{sh})$ and velocity $(v_{sh})$ of the inner shell are found to be strongly correlated through conservation of energy and momentum. Processes such as turbulent mixing and reverse shocks cause the thickness $(\Delta R_{sh})$ of the inner shell to remain constant once it has begun to coast (defined to begin at radius, $R_{sh,0}$). A detailed description of the formation of the inner shell as well as emission methodology used in this work can be found in Paper I. The velocity of the inner shell that we found as a fit parameter in Paper I was approximately 10% of our theoretically predicted value. Upon revisiting our derivation of R band luminosity used in Paper I, we found that there was a missing factor of $\pi$ and with this small correction the inner shell velocity used in this work is now in full agreement with the theoretical value (see equation 7 of Paper I).

The inner shell is fully parameterized by: temperature, mass, velocity, thickness and coasting radius. The mass and velocity are determined through conservation of energy and momentum, the derivation of the formulae used to describe these parameters can be found in Paper I (equations 6 and 7 respectively). For the analysis of each SLSN target considered in this work we use the same coasting radius for the inner shell, namely the best fit value of $R_{sh,0} = 4 \times 10^{14}$ cm that was found in Paper I. The only parameter pertaining solely to the inner shell that we allow to be adjusted is the shell thickness.

A detailed look at the formation of the inner shell using a full hydrodynamic treatment would help to understand how physical parameters of the inner shell are affected by changing initial conditions such as the time delay between SN and QN.

### 4.2. *The Envelope*

Fiducial values, found in Paper I, for the shock speed $(v_{shock} = 6000$ km s$^{-1})$ and the outer edge velocity of the homologously expanding $(v \propto r)$ envelope $(v_{SN,max} = 4100$ km s$^{-1})$ are used for the work presented here. By fixing $v_{shock}$ and $v_{SN,max}$ the variation in the time at which the *cooling* phase begins is uniquely determined by $t_{delay}$. Following the same methodology as Paper I, a simple temperature profile is considered for the envelope where $T(r) \propto r^{-\beta}$ with $\beta = 0.2$. In this work the progenitor star mass $(M_\star)$ is a free parameter and the mass of the inner shell $(M_{sh})$ is prescribed by conservation laws; thus the mass of the envelope is found simply as $M_{env} = M_\star - M_{sh}$.

### 4.3. *Cooling*

Since the inner shell and the envelope are initially both parts of the same physical structure, namely the re-shocked SN envelope, they both start with same initial temperature $(T_0)$. As the envelope and the inner shell expand they cool adiabatically; due to the difference in geometries (the envelope expanding spherically and the inner shell with constant thickness) they follow different cooling profiles. The temperature of the envelope evolves as $T_{env}(t) \propto T_0 \, t^{-2}$ and that of the inner shell as $T_{sh}(t) \propto T_0 \, t^{-4/3}$ (see Paper I for derivation).

As continuum radiation is emitted by the envelope an equivalent amount of thermal energy is removed, thereby conserving energy. Since the *cooling* phase begins when the envelope is still relatively optically thick, radiative cooling starts at the outer edge of the envelope. Due to radiative cooling, over time a hot-cold interface progresses inward through the envelope. In our model once an outer layer of the envelope is radiatively cooled it no longer emits radiation. At the late stages of the dsQN light curve, radiative cooling will have caused the hot-cold interface to progress and most of the envelope will have cooled. By this time the envelope has also expanded causing it to become more optically thin and thus making our optically thick radiative cooling approximation less valid. In reality as the envelope becomes more diffuse radiative cooling will cause the whole envelope to cool rather than just the outer layers, and will lead to an increase in the cooling rate of the envelope with time. The effect of this can be seen in the envelope contribution to the dsQN light curve (plotted as a blue dotted line in Figure 1): as the change in slope around Day 170 is due to the envelope remaining hotter than is physically likely. Since the envelope is optically thin when this cooling artefact becomes significant, in most cases the luminosity from the inner shell will already dominate the overall light curve rendering the problem moot. Rather than adding a more complicated radiative cooling law to our model we will simply note when the effect is seen during our fits to observations.

### 5. MODEL

For this work we use the astrophysical modelling software SHAPE, which allows us to construct the 3-D geometry of the dsQN scenario and perform radiative
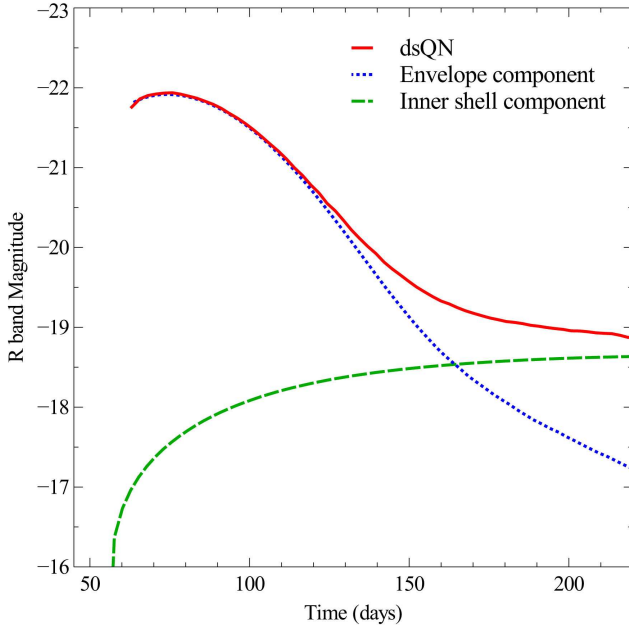
Fig. 1. Plotted as a red solid line is the $R$-band light curve of the dsQN. Radiation from the two components of the dsQN are also plotted. Radiation from the envelope is represented by the blue dashed line and that from the inner shell is denoted by the green dotted line. The color figure can be viewed online.
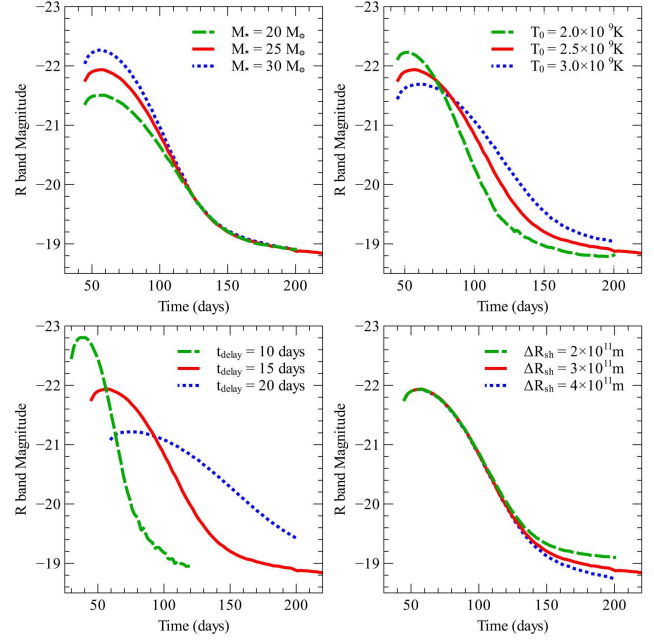


Fig. 2. In each panel the overlay of the $R$-band light curve of dsQN models with three different sets of physical parameters is plotted. For each panel one physical parameter is varied while the remaining parameters are held constant (values given in text). Top-left: *Mass of envelope ($M_\star$)*. $M_\star = 20\,M_\odot$ (green dashed line), $M_\star = 25\,M_\odot$ (red solid line) and $M_\star = 30\,M_\odot$ (blue dotted line). Top-right: *Initial shock temperature ($T_0$)*. $T_0 = 2 \times 10^9$ K (green dashed line), $T_0 = 2.5 \times 10^9$ K (red solid line) and $T_0 = 3 \times 10^9$ K (blue dotted line). Bottom-left: *Time delay between SN and QN ($t_{\rm delay}$)*. $t_{\rm delay} = 10$ days (green dashed line), $t_{\rm delay} = 15$ days (red solid line) and $t_{\rm delay} = 20$ days (blue dotted line). Bottom-right: *Inner shell thickness ($\Delta R_{\rm sh}$)*. $\Delta R_{\rm sh} = 2 \times 10^{11}$m (green dashed line), $\Delta R_{\rm sh} = 3 \times 10^{11}$m (red solid line) and $\Delta R_{\rm sh} = 4 \times 10^{11}$m (blue dotted line). The color figure can be viewed online.

transfer (Wenger et al. 2012). The temperature as well as the dimensions of the geometry are governed by the physics described in § 4.

### 5.1. Radiative Transfer Parameters

For this analysis, the radiative transfer calculation follows the same methodology used in Paper I in which for each frequency ($\nu$) an emission and absorption coefficient are specified. The emission coefficient used for the envelope has the form

$$j_\nu = \frac{A\,n_{\rm e}^2}{T^{3/2}} e^{h\nu/kT},\qquad(1)$$

where $A$ is a multiplicative factor is related to the underlying radiative process. For this analysis we chose to fix $A$ over the filter passband of each studied SLSN. For the $R$ band $A = 5\times10^5$, for the $V$ band $A = 1\times10^6$, for the $B$ band $A = 7\times10^4$, and for the $u$ band $A = 5\times10^5$. The variations required in $A$ allude to an emission mechanism more complex than our approximation described by equation 1. Assuming local thermodynamic equilibrium the absorption coefficient corresponding to our $j_\nu$ is found by means of the Planck function ($B_\nu$) to be

$$k_\nu = \frac{j_\nu}{B_\nu}.\qquad(2)$$

We as well include a Thompson scattering term to equation 2 of the form

$$k_{\nu,\rm TH} = B\,n_{\rm e}\,\sigma_{\rm TH},\qquad(3)$$

where $\sigma_{\rm TH}$ is the Thompson scattering cross-section and $B$ is a multiplicative factor which represents the fraction of scattered light that is not scattered back into the beam. For this work we set $B = 5 \times 10^{-4}$, which is the same as that used in Paper I. Further details on SHAPE and the radiative transfer calculation can be found in Paper I.

### 5.2. Fiducial Model Characteristics

Before fitting the observed SLSNe light curves with the dsQN model we felt it would be informative to explore the light curves of dsQNe in a more general sense. To this end we built a generic dsQN model with the following physical parameters: $M_\star = 25\,M_\odot$, $T_0 = 2.5 \times 10^9$ K, $\Delta R_{\rm sh} = 3 \times 10^{13}$cm and $t_{\rm delay} = 15$ days. The light curve associated with this model is
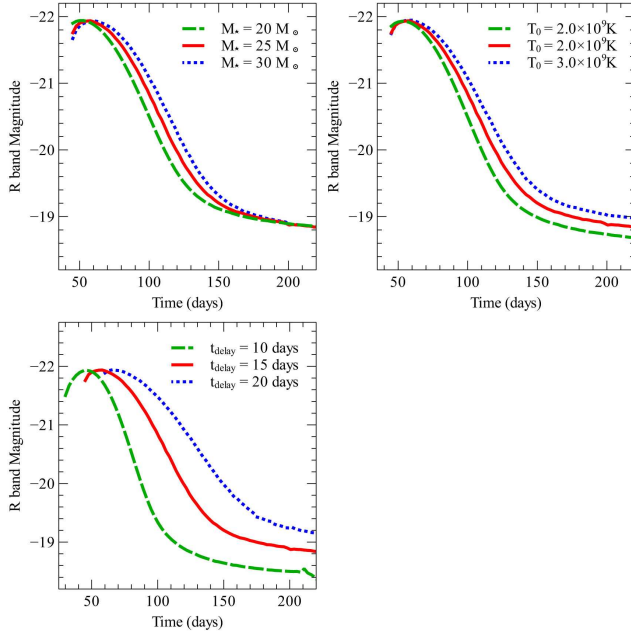
Fig. 3. In each panel the overlay of the $R$-band light curve of dsQN models with three different sets of physical parameters is plotted. Each light curve is scaled using the radiative transfer parameter $A$ such that the peaks reach the same absolute magnitude. For each panel one physical parameter is varied while the remaining parameters are held constant (values given in text). Top-left: *Mass of envelope* ($M_\star$). $M_\star = 20\,M_\odot$ (green dashed line), $M_\star = 25\,M_\odot$ (red solid line) and $M_\star = 30\,M_\odot$ (blue dotted line). Top-right: *Initial shock temperature* ($T_0$). $T_0 = 2 \times 10^9$ K (green dashed line), $T_0 = 2.5 \times 10^9$ K (red solid line) and $T_0 = 3 \times 10^9$ K (blue dotted line). Bottom-left: *Time delay between SN and QN* ($t_{\mathrm{delay}}$). $t_{\mathrm{delay}} = 10$ days (green dashed line), $t_{\mathrm{delay}} = 15$ days (red solid line) and $t_{\mathrm{delay}} = 20$ days (blue dotted line). The color figure can be viewed online.

plotted as a red solid line in Figure 1. The component of the light curve caused by emission from the envelope is plotted as a blue dotted line in Figure 1 and the contribution from the inner shell is represented by the green dashed line. As can be seen in Figure 1 the broad peak in the dsQN light curve is due to radiation emitted from the envelope. As time progresses the envelope cools and becomes less dense causing a rapid drop in emission. This allows for radiation from the slowly coasting and thus slowly cooling inner shell to begin to shine through. The post-peak luminosity decay rate in the overall light curve of the dsQN is slowed due to emission from the inner shell. In the late stages of the dsQN light curve there can exist a plateau due to emission from the inner shell.

In this section we will investigate the effect on light curve morphology of varying the physical parameters of a dsQN. For comparative purposes in each of the panels in Figure 2 the red solid line denotes the same light curve as the overall light curve seen in Figure 1

(red solid line). Then in each panel of Figure 2 one physical parameter is adjusted to show its effect on the light curve; the higher value is denoted by the blue dotted line and the lower value by the green dashed line. Clock-wise starting from the upper-left panel of Figure 2 we show effect of varying $M_\star$ ($20\,M_\odot$, $25\,M_\odot$ and $30\,M_\odot$), varying $T_0$ ($2 \times 10^9$K, $2.5 \times 10^9$K and $3 \times 10^9$K), varying $\Delta R_{\mathrm{sh}}$ ($2 \times 10^{13}$cm, $3 \times 10^{13}$cm and $4 \times 10^{13}$cm) and varying $t_{\mathrm{delay}}$ (10 days, 15 days and 20 days).

As seen in the upper-left panel of Figure 2 the effect of varying $M_\star$ is simply to scale the height of the peak, with higher masses yielding a higher peak. As the post-peak luminosity drops support by radiation from the underlying inner shell kicks in at the same time for each of the light curves. This convergence is caused by the fact that changing the mass of the envelope has no effect on the emission from the inner shell.

Changing $T_0$ of the dsQN (as seen in the upper-right panel of Figure 2) as well acts to scale the height of the peak; however, the height of the peak is inversely proportional to $T_0$ (due to the form of the emission coefficient, see equation 1). In the case of varying $T_0$ the support from the inner shell on the overall light curve begins at different times because the temperature directly effects the amount of radiation that can be emitted by the inner shell. For higher $T_0$ the luminosity of the inner shell is greater and its effect on the overall light curve can be seen sooner.

As shown in Figure 1 the effect on the dsQN light curve of radiation from the inner shell can only be seen in the late stages, once emission from the envelope has faded sufficiently. Thus as expected the lower-right panel of Figure 2 shows that changing $\Delta R_{\mathrm{sh}}$ only impacts the tail of the dsQN light curve. All things being equal, a thinner shell implies a higher density and thus more intense emission from the inner shell. The effect of increased density causing increased radiation can be seen in the lower-right panel on Figure 2 where the thinner $\Delta R_{\mathrm{sh}}$ light curve has a more prominent plateau.

The physical parameter that has the most dramatic effect on light curve morphology is $t_{\mathrm{delay}}$, which can be seen in the lower-left panel of Figure 2. A shorter $t_{\mathrm{delay}}$ implies that the SN envelope is more dense when it is re-shocked, which translates into a higher peak in the light curve. The shorter $t_{\mathrm{delay}}$ also demands that the SN envelope be smaller when it is re-shocked, leading to significant adiabatic losses and a steep luminosity decay rate. The dsQN with a longer $t_{\mathrm{delay}}$ cannot achieve as high a luminosity peak. However, reduced adiabatic losses allow the light curve to remain at a higher relative brightness for a longer time when compared to a dsQN with a shorter $t_{\mathrm{delay}}$. Another effect of adjusting $t_{\mathrm{delay}}$ is to change the time of peak luminosity relative to the time of SN explosion. A longer $t_{\mathrm{delay}}$ dsQN will
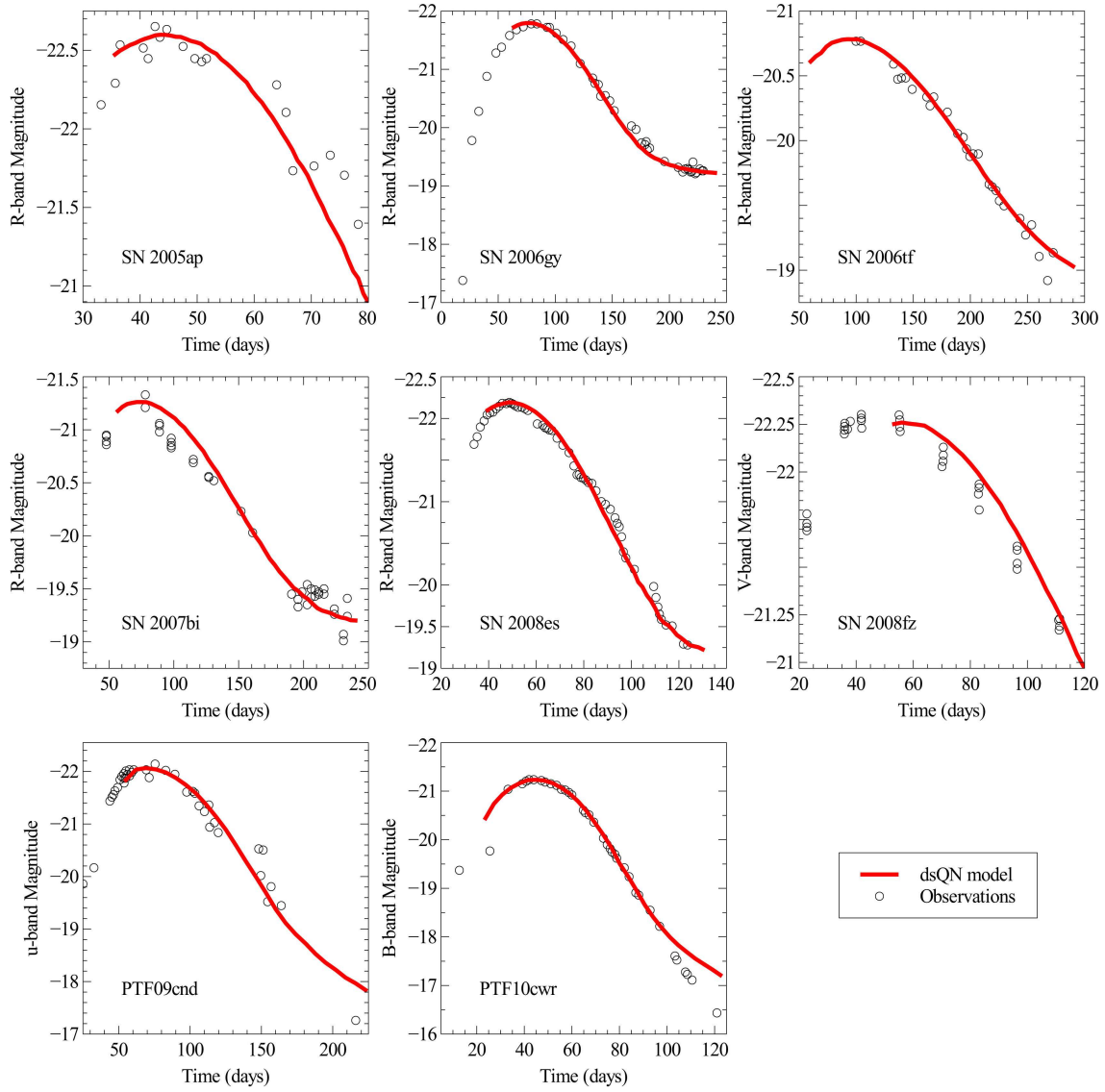
Fig. 4. For each panel the observed light curve is plotted with open black circles and the dsQN model is plotted as a solid red line. Time since the inferred SN explosion is plotted along the horizontal axis and the absolute magnitude in the observed band is plotted on the vertical axis. The best fit parameters used to generate these fits can be found in Table 3. From left-to-right and top-to-bottom the panels represent: SN 2005ap, SN 2006gy, SN 2006tf, SN 2007bi, SN 2008es, SN 2008fz, PTF09cnd and PTF10cwr. The color figure can be viewed online.

peak in brightness later in time due to the simple fact that the shock must traverse a larger envelope before it can break out.

From Figure 2 it is clear that changing the values of $M_\star$, $T_0$ or $t_{delay}$ all effect the height of the luminosity peak of the light curve of a dsQN. Our approximated emission coefficient (see equation 1) contains the free parameter $A$ which as well directly effects the amount of radiation emitted in our model at any given time. Thus we can use $A$ to gain a better visualization of the effect that changing each physical parameter ($M_\star$, $T_0$ and $t_{delay}$) has on the shape of the light curve. In Figure 3 we perform the same comparison as shown

in Figure 2 with the addition that each light curve is rescaled using $A$, so that the absolute magnitude of the light curve in the $R$ band peaks at $-22$. By comparing the light curves in the upper two panels of Figure 3 it is clear that neither changing $M_\star$ nor $T_0$ significantly affects the post-peak luminosity decay rate of the dsQN. As seen in the upper-left panel of Figure 3 increasing the mass of the envelope marginally increases the breadth of the light curve peak, but does not affect the slope. Turning to the upper-right panel of Figure 3, one can see that increasing $T_0$ has the same effect on the morphology of the light curve peak as increasing $M_\star$. The only difference between adjusting $M_\star$ and

$T_0$ is that the intensity of the radiation from the inner shell increases with $T_0$ causing the plateau to vary directly with $T_0$.

From Figures 2 and 3 we can see that varying $T_0$ and $M_\star$ effectively acts only as a scaling, with minimal effect on the luminosity decay rate of the light curve. Since the effect is virtually the same, for all our fits to observed SLSN light curves we choose to fix $T_0$ at $2.5 \times 10^9$ K and allow $M_\star$ to vary. The lower-left panel of Figure 3 displays the effect of varying the delay between SN and QN. As was shown in Figure 2 increasing $t_{\mathrm{delay}}$ causes the peak luminosity to occur later with respect to the time of SN explosion. Another consequence of increasing $t_{\mathrm{delay}}$ is to slow down the luminosity decay rate of the post-peak light curve of a dsQN. As we have found in this analysis the only parameter that we can adjust in order to change the luminosity decay rate in the dsQN model is $t_{\mathrm{delay}}$.

## 6. FITS TO OBSERVATIONS

For this work we have fit the light curve of eight SLSNe using the dsQN model. The parameters that we adjusted to fit each set of observations were; $t_{\mathrm{delay}}$, $\Delta R_{\mathrm{sh}}$ and $M_\star$. Of these three free parameters $t_{\mathrm{delay}}$ and $M_\star$ only significantly affect the radiation from the envelope while $\Delta R_{\mathrm{sh}}$ only affects the emission from the inner shell. As was shown in § 5.2, varying $M_\star$ or $T_0$ have the same effect on the dsQN light curve. Thus for simplicity we fixed $T_0 = 2.5 \times 10^9$ K and allowed $M_\star$ to vary between model fits. The best fit values of these parameters for each SLSNe surveyed can be found in Table 3. For each panel of Figure 4 the observations are plotted with open circles and the best fit dsQN light curve is plotted as a red solid line. Figure 5 displays each of the best fit dsQN light curves plotted on the same axes. From Figure 5 it can be seen that for dsQNe in which an inner shell is formed (all but PTF09cnd and PTF10cwr) the magnitude of the radiation from the inner shell is remarkably consistent.

### 6.1. SN 2005ap

The best fit progenitor mass for SN 2005ap was $28\,M_\odot$. The high peak absolute magnitude and fast luminosity decay rate of SN 2005ap required a short time delay ($t_{\mathrm{delay}} = 11.25$ days) dsQN to fit the observations (see top row left panel of Figure 4). Since the observations of SN 2005ap were only carried out for approximately 35 days post-peak, the luminosity had not dropped enough to potentially see a contribution from the inner shell. Thus we were unable to determine if an inner shell was present in the dsQN model of this SLSN.

### 6.2. SN 2006gy

In the proof-of-principle paper (Ouyed et al. 2012) the fits to SN 2006gy ignored a $\pi$ factor in the $R$ band magnitude calculation. The fits presented here take

this into account and thus are more accurate. Our fit to the observed light curve of SN 2006gy is displayed in the top row middle panel of Figure 4. A $30\,M_\odot$ progenitor star was used in our model and the broad peak of SN 200gy required a time delay of 17 days. The distinct plateau in the late stages of the light curve was fit using a inner shell $2 \times 10^{13}$cm thick.

### 6.3. SN 2006tf

Although the observations of SN 2006tf do not include the leading edge of the light curve, the slow luminosity decay rate demanded that the dsQN used in this fit have the longest time delay of all SLSNe modelled in this work ($t_{\mathrm{delay}} = 22.5$ days). A progenitor star of $26\,M_\odot$ was used in our fit and the late stages of the light curve are affected by the contribution from an $4 \times 10^{13}$cm thick inner shell. Our fit to the observed light curve of SN 2006tf is found in the top row right panel of Figure 4.

### 6.4. SN 2007bi

A plot of our fit to the light curve of SN 2007bi is displayed in the middle row left panel of Figure 4. A progenitor star of $25.5\,M_\odot$ was used in our model and the delay between SN and QN that best fitted the shape of the SN 2007bi light curve was $t_{\mathrm{delay}} = 18.5$ days. The late stage plateau of the light curve was fit in our dsQN model by radiation predominantly from a $2.5 \times 10^{13}$cm thick inner shell.

### 6.5. SN 2008es

The narrow peak of the light curve of SN 2008es was fit by dsQN of a $28\,M_\odot$ progenitor star with a time delay between SN and QN of 12.5 days. Approximately 100 days after the SN explosion the light curve of SN 2008es begins to be supported by luminosity originating from a $3 \times 10^{13}$cm thick inner shell. A plot of our fit to the light curve of SN 2008es is displayed in the middle row, middle panel of Figure 4.

### 6.6. SN 2008fz

The combination of high peak luminosity and broad light curve of SN 2008fz required a $35\,M_\odot$ progenitor star and time delay of 20 days between SN and QN. Our dsQN fit to the light curve is found in the middle row middle panel of Figure 4. The late stages of the SN 2008fz light curve are supported by luminosity from a $5 \times 10^{12}$cm inner shell.

### 6.7. PTF09cnd

A plot of our fit to the light curve of PTF09cnd is displayed in the bottom row, left panel of Figure 4. The best fit parameters for PTF09cnd ($t_{\mathrm{delay}} = 17$ days and $M_\star = 31\,M_\odot$) are similar to those of SN 2006gy with one exception. For PTF09cnd we found that the inner shell had to be nearly 10 times thicker than that of SN 2006gy ($2 \times 10^{14}$ cm, or approximately two fifths

TABLE 3

COMPARISON OF DSQN MODEL PARAMETERS USED TO FIT EACH SLSNE.

| SLSNe | Time Delay ($t_{\mathrm{delay}}$) [days] | Mass ($M_\star$) [$M_\odot$] | Shell Thickness ($\Delta R_{\mathrm{sh}}$) [$10^{13}$ cm] |
|---|---|---|---|
| SN 2005ap | 11.25 | 28 | N/A |
| SN 2006gy | 17.0 | 30 | 2.0 |
| SN 2006tf | 22.5 | 26 | 4.0 |
| SN 2007bi | 18.5 | 25.5 | 2.5 |
| SN 2008es | 12.5 | 28 | 3.0 |
| SN 2008fz | 20.0 | 35 | 0.5 |
| PTF09cnd | 17.0 | 31 | $\gtrsim 20$ |
| PTF10cwr | 7.5 | 25 | N/A |
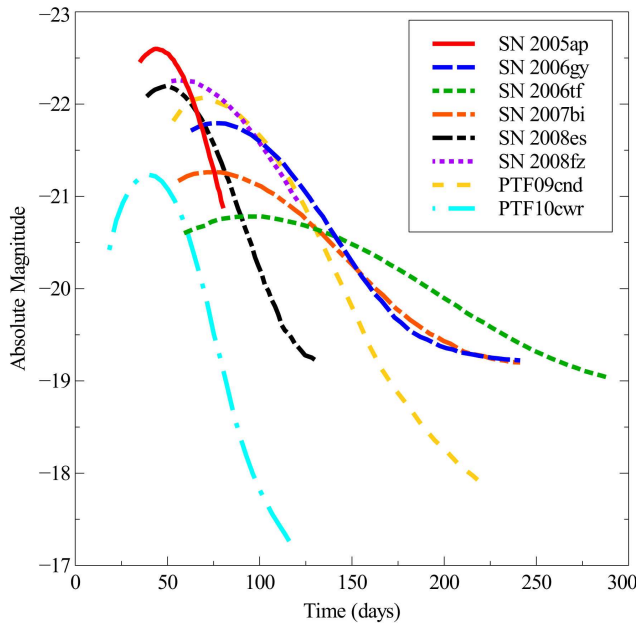
Fig. 5. The best fit dsQN model light curve for each of the SLSNe studied in this work are plotted on the same axis. The color figure can be viewed online.

of the initial radius of the inner shell) in order to fit the late stages of the light curve. This difference in inner shell geometry may be attributed to a difference in the abundance of the inner SN envelope and higher order mixing effects related to specific dynamics of the QN/SN interaction. Another possible explanation for the reduced radiation from the inner shell at the late stages of the light curve of PTF09cnd is that the inner shell is cooling faster than the imposed $T \propto t^{-4/3}$ law. A larger cooling index would simply imply that the shell is expanding in thickness with time. A more detailed study of the hydrodynamics of the QN/SN interaction would help to further understand the formation process of the inner shell. The late stages of

our dsQN model fit to PTF09cnd displays a change in slope which is an artifact of the radiative cooling approximation discussed in § 4.3.

### 6.8. *PTF10cwr / SN 2010gx*

Displayed in the bottom row middle panel of Figure 4 is the dsQN model fit to the observed light curve of PTF10cwr. This SLSN displayed the narrowest light curve of all those studied in this work and thus was fit with the shortest time delay (7.5 days) dsQN. A 25 $M_\odot$ progenitor star was used in our best fit model and the light curve of PTF10cwr showed no sign of the presence of an inner shell. The late stages of our dsQN model fit to PTF10cwr displays a change in slope which is an artifact of the radiative cooling approximation discussed in § 4.3.

### 7. DISCUSSION

#### 7.1. *Spectra*

In the case of SN 2006gy there exist numerous observations that detail its spectral evolution (Smith et al. 2010). Unfortunately for other SLSNe, the study of the spectra is limited by the number of observations available, which in many cases is one spectral observation around the time of peak brightness. As discussed in Paper I, the dsQN can display an H$\alpha$ signature in which the underlying broad structure of the line is caused by thermally broadened emission originating from the inner shell, and emission and absorption from the envelope result in a blue-side absorption feature. Figure 6 displays a schematic representation of the line of sight evolution of the H$\alpha$ line in a typical dsQN. Unique to the dsQN scenario, the wings of the H$\alpha$ line are caused by thermal broadening rather than velocity broadening (see right-most H$\alpha$ line in Figure 6), naturally accounting for the long-lasting breadth of the line. As the H$\alpha$ line progresses through the hot component of the envelope, a P Cygni profile is added to the structure of the line. This is displayed as the middle H$\alpha$ line in Figure 6. Finally the cold outer layer
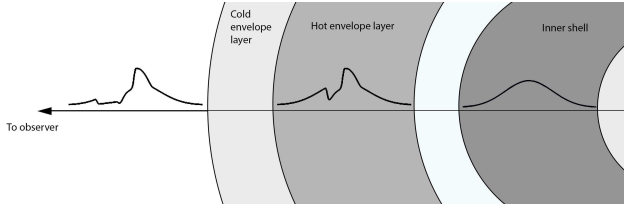
Fig. 6. The three Hα emission lines plotted here represent the Hα line at three different stages of its line of sight evolution. In the background a not-to-scale cartoon representation of the physical structure that contributes to the given emission line. The far right Hα line is thermally broadened emission from only the inner shell. The broad structure of the middle Hα line is emission from only the inner shell, while the hot envelope contributes a P Cygni profile on top of the broad structure. The far left Hα line is emission from the entire dsQN along the line of sight. The radiatively cooled outer layer adds increased blue-side absorption in the Hα line.

of the envelope adds absorption to the blue-side of the Hα line (seen as the left-most line plotted in Figure 6).

According to their classification, SN 2005ap, PTF09cnd and PTF10cwr do not display any prominent hydrogen lines, although each of these SLSNe do show some indication of a weak Hα line near peak luminosity, as mentioned in the supplemental material associated with Quimby et al. (2011). Unfortunately the poor signal to noise (S/N) ratio eliminates any possibility of studying these weak lines. The two spectral observations of SN 2008fz each show a strong Hα line that resembles that of SN 2006gy (Drake et al. 2010). While the Hα lines display a broad underlying structure, the only spectral observation of SN 2008fz that is at an epoch which would show significant absorption by the envelope has the red-wing of the Hα line cut off. Without the red-side of the line there is no way of comparing the observations to our predicted dsQN Hα line. The spectra of SN 2008es contain broad Balmer lines which display a P Cygni profile. However, the poor S/N ratio of the observations inhibits any study of these lines (Gezari et al. 2009).

For our work in Paper I we performed detailed analysis of the spectral evolution of the Hα line observed in SN 2006gy. The dsQN model was shown to provide a unique explanation for both the persistent broad structure of the line as well as the blue-side absorption feature seen in Hα of SN 2006gy. In this work we study the Hα line of two other SLSNe; SN 2006tf and SN 2007bi. For SN 2007bi the Hα line observed in the spectrum 54 days after peak brightness (see upper left panel of Figure 7) is mysterious as all other features of the spectrum are consistent with a type Ic SN and thus should be free of hydrogen (Gal-Yam et al. 2009). For comparative purposes we have plotted the Hα line observed in SN 2006gy (upper right panel of Figure 7) from a similar epoch as the spectral observation of SN 2007bi.



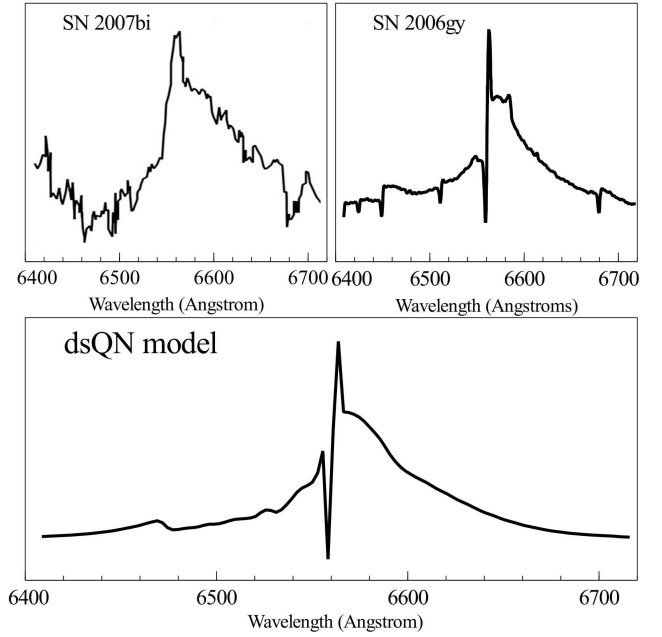Fig. 7. Comparison of Hα line from spectra of SN 2006gy, SN 2007bi and the dsQN model. Top-Left: Plotted is the observed Hα line of SN 2007bi approximately 54 days after peak luminosity. Data from Gal-Yam et al. (2009). Top-Right: The Hα line from the spectrum of SN 2006gy observed at approximately 50 days post-peak luminosity. Data from Smith et al. (2010). Bottom: The dsQN model Hα line 50 days post-peak luminosity, from Paper I.

The bottom panel of Figure 7 is the dsQN model Hα line for the same epoch (from Paper I). Although the S/N ratio of the SN 2007bi prevents the study of the delicate structure of the Hα line the large scale features are similar to those of a dsQN, namely the broad underlying structure and strong blue-side absorption.

The spectrum of SN 2006tf has multiple observations at different epochs along its light curve. As noted by Smith et al. (2008) the Hα line observed in SN 2006tf resembles that of SN 2006gy as it contains a broad underlying structure that becomes more prominent with time. The upper left panel of Figure 8 displays an overplot of four observations of the Hα line of SN 2006tf. For comparison the upper right panel of Figure 8 displays an overplot of four spectral observations of SN 2006gy for similar epochs. The bottom panel of Figure 8 displays dsQN model Hα lines from roughly similar epochs as the observations of SN 2006tf and SN 2006gy. In the dsQN model Hα line and that of SN 2006tf and SN 2006gy there exists a broad component to the line as well as a blue-side absorption feature that diminishes in strength over time.

The differences in the Hα lines of SN 2006tf and SN 2007bi are consistent with the different $t_{\rm delay}$ of the dsQN description of these SLSNe. In the case of SN 2007bi the shorter time delay ($t_{\rm delay} = 18.5$ days) implies that the envelope is still dense at the time of
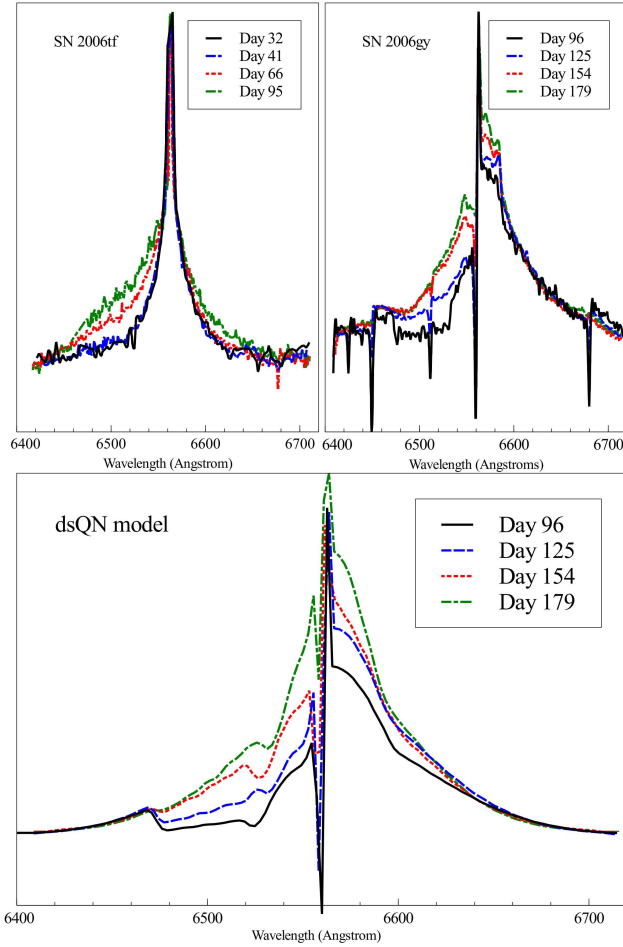
Fig. 8. Comparison of evolution of Hα line from SN 2006tf spectra, SN 2006gy and our dsQN model Hα line evolution. Top-Left: Plotted is an overlay of spectral observations of the Hα line of SN 2006tf. Data from Smith et al. (2008). The observations are from; 32 days (black solid line), 41 days (blue dash line), 66 days (red dotted line) and 95 days (green dash-dot line) after the first observation. Top-Right: An overlay of Hα spectral lines from SN 2006gy is plotted, data from Smith et al. (2010). The Hα lines plotted are from 96 days (black solid line), 125 days (blue dashed line), 154 days (red dotted line) and 179 days (green dash-dot line) after the inferred SN explosion date. Bottom: Plotted is an overlay of the dsQN model Hα line that was used to fit the observations of SN 2006gy in Paper I. The Hα lines plotted are from days; 96 (black solid line), 125 (blue dashed line), 154 (red dotted line) and 179 (green dash-dot line) after the inferred SN explosion date. The color figure can be viewed online.

the spectral observation and thus there exists a strong blue-side absorption feature. As for SN 2006tf, the time delay is significantly longer ($t_{\mathrm{delay}} = 22.5$ days). Therefore, the envelope is much more diffuse during the spectral observations and the blue-side absorption feature is weaker.

Interestingly the SLSNe with light curves that are best fit with dsQN models without inner shells

(SN 2005ap and PTF10cwr), or with minimal influence from the inner shell (PTF09cnd), show no broad Hα features in late phase spectral observations (see supplemental material from Quimby et al. 2011). This is consistent with the dsQN explanation for the origin of the persistent broad Hα feature.

### 7.2. The Envelope

The mass of the envelope as well as the initial shock temperature both act only to scale up or down the peak of the dsQN light curve. We found that the only parameter capable of significantly changing the luminosity decay rate is the time delay between SN and QN. All SLSNe with X-ray observations show remarkably quiet X-ray production. This is expected in the context of a dsQN due to the cold outer layer of the envelope which would act as an efficient absorber of high energy radiation. The formulation that we used for the radiative transfer coefficients (see equations 1 and 2) provided a good fit to each of the SLSN light curves that we studied. This could be an indication that the continuum emission mechanism for these SLSNe resembles recombination, which has a similar form as equation 1. Further study of SLSNe in which the light curve is observed in several passbands would help to determine the true temperature dependence of the emission coefficient and help in understanding the radiation mechanism.

### 7.3. The Inner Shell

The luminosity from the inner shell only begins to affect the shape of the light curves well past peak luminosity (typically once the luminosity has dropped to $\approx -19.5$ absolute magnitude). The slowing of the luminosity decay rate, or *plateauing* of the light curve in the late stage is caused by radiation from the inner shell shining through the diffuse envelope.

### 8. CONCLUSIONS AND PREDICTIONS

We have shown that the dsQN scenario can be used to explain the light curves of all eight SLSN targets studied. In the context of dsQNe, progenitor stars ranging between 25–35 $M_\odot$ provide ample energy to power the large radiated energy budget of SLSNe.

We found that the physical parameter with the greatest impact on dsQN light curve morphology was the time delay between SN and QN. Shorter time delay dsQN yield a peak magnitude that is brighter and a faster luminosity decay rate (narrower light curve). While for longer time delays the peak magnitude is dimmer and the light curve is broader. A variation in time delay in the dsQN description provides an explanation for the wide variety of SLSN light curve morphologies. From our analysis we found that for shorter time delay dsQN the inner shell may not be formed.

The implication is that the energy that would go into forming the inner shell may instead be lost to pressure-volume work. However, further study of the dynamics of the QN-SN interaction must be undertaken.

We have also examined the singular H$\alpha$ spectral line profile found in three different SLSNe observations (SN 2006gy, SN 2006tf and SN 2007bi). The broad structure of the line is accounted for by thermally broadened emission from the inner shell, while the intermediate peak and the blue-side absorption feature are due to contribution from the envelope. We found that the evolution of the blue-side absorption feature in the H$\alpha$ line of SN 2006gy and SN 2006tf is consistent with diffusion of the envelope.

Unique to the dsQN scenario is the fact that any core collapse SN that leaves behind a massive neutron star can in turn undergo a QN explosion. This is due to the fact that the conditions of the interior of the progenitor star determine whether the neutron star could become susceptible to QN collapse. There is no correlation with to the progenitor star envelope (for example whether or not hydrogen is present). Thus we expect a wide variety of types of SN can become super-luminous due to re-brightening via a QN collision.

A distinguishing feature predicted by the dsQN model is a unique chemical abundance caused by the spallation of the SN envelope by the QN ejecta (Ouyed et al. 2011a). Recent observations have suggested that plausible signs of the QN were found in Cas A (Hwang & Laming 2012). As described in Ouyed et al. (2011a) the layer of the SN envelope undergoes spallation by the QN ejecta depending on the density of the envelope at the moment of impact. For a shorter time delay QN the Ni layer would be destroyed in favor of the production of sub-$^{56}$Ni elements such as; Ti, V, Cr and Mn (Ouyed et al. 2011a). This process should also lead to mixing that would cause Fe to be found in the outer regions of a dsQN remnant (Ouyed et al. 2011a). The formation of $^{44}$Ti at the expense of $^{56}$Ni will play an important role in the very late stage ($t \approx 1000$ days) luminosity of dsQN. For longer time delay QN the spallation process occurs in the carbon & oxygen layer of the SN envelope which leads to a unique chemical signature of the dsQN. Spallation of the carbon & oxygen layer would lead to an over-abundance of lithium in the dsQN remnant (Ouyed 2013).

A dsQN is expected to emit two bursts of X-rays. The first X-ray emission event would occur when the shock from the original SN breaks out of the stellar envelope and the second would occur at the QN shock break-out of the SN envelope. If the time delay between SN and QN is short then the X-ray bursts could in fact overlap, leading to a broadened X-ray light curve. However if the time delay is long then there should be two distinct X-ray peaks.

## REFERENCES

Alcock, C., Farhi, E., & Olinto, A. 1986, ApJ, 310, 261

Arnett, W. D. 1982, ApJ, 253, 785

Berezhiani, Z., Bombaci, I., Drago, A., Frontera, F., & Lavagno, A. 2003, ApJ, 586, 1250

Blinnikov, S. I. 2008, in AIP Conf. Ser. 1016, Origin of Matter and Evolution of Galaxies, ed. T. Suda, T. Nozawa, A. Ohnishi, K. Kato, M. Y. Fujimoto, T. Kajino, & S. Kubono (Melville, NY: AIP), 241

Bodmer, A. R. 1971, Phys. Rev. D, 4, 1601

Bombaci, I. & Datta, B. 2000, ApJ, 530, L69

Bucciantini, N., Quataert, E., Metzger, B. D., Thompson, T. A., Arons, J., & Del Zanna, L. 2009, MNRAS, 396, 2038

Cheng, K. S. & Dai, Z. G. 1996, Phys. Rev. Lett., 77, 1210

Chevalier, R. A. 1982, ApJ, 258, 790

————. 2012, ApJ, 752, L2

Chevalier, R. A. & Irwin, C. M. 2011, ApJ, 729, L6

————. 2012, ApJ, 747, L17

Dai, Z., Peng, Q., & Lu, T. 1995, ApJ, 440, 815

Dessart, L., Hillier, D. J., Waldman, R., Livne, E., & Blondin, S. 2012, MNRAS, 426, L76

Drake, A. J., et al. 2009, ApJ, 696, 870

Drake, A. J., et al. 2010, ApJ, 718, L127

Fryer, C. L. 1999, ApJ, 522, 413

Gal-Yam, A., et al. 2009, Nature, 462, 624

Gezari, S., et al., 2009, ApJ, 690, 1313

Ginzburg, S., & Balberg, S. 2012, ApJ, 757, 178

Grassberg, E. K., Imshennik, V. S., & Nadyozhin, D. K. 1971, Ap&SS, 10, 28

Hwang, U. & Laming, J. M. 2012, ApJ, 746, 130

Itoh, N. 1970, Prog. Theor. Phys., 44, 291

Kasen, D., & Bildsten, L. 2010, ApJ, 717, 245

Kasen, D., Woosley, S. E., & Heger, A. 2011, ApJ, 734, 102

Kawabata, K. S., Tanaka, M., Maeda, K., Hattori, T., Nomoto, K., Tominaga, N., & Yamanaka, M. 2009, ApJ, 697, 747

Keränen, P., Ouyed, R., & Jaikumar, P. 2005, ApJ, 618, 485

Kiewe, M., et al. 2012, ApJ, 744, 10

Koning, N., Ouyed, R., & Leahy, D. 2012, ArXiv:1205.4355 [astro-ph.HE]

Law, N. M., et al. 2009, PASP, 121, 1395

Leahy, D., & Ouyed, R. 2008, MNRAS, 387, 1193

Miller, A. A., et al. 2009, ApJ, 690, 1303

Moriya, T. J., Blinnikov, S. I., Tominaga, N., Yoshida, N., Tanaka, M., Maeda, K., & Nomoto, K. 2013, MNRAS, 428, 1020

Niebergal, B., Ouyed, R., & Jaikumar, P. 2010, Phys. Rev. C, 82, 062801

Olinto, A. V. 1987, Phys. Lett. B, 192, 71

Ouyed, R. 2013, MNRAS, 428, 236

Ouyed, R., Dey, J., & Dey, M. 2002, A&A, 390, L39

Ouyed, R., Kostka, M., Koning, N., Leahy, D. A., & Steffen, W. 2012, MNRAS, 3043 (Paper I)

Ouyed, R., & Leahy, D. 2009, ApJ, 696, 562

Ouyed, R., Leahy, D., & Niebergal, B. 2007a, A&A, 473, 357

————. 2007b, A&A, 475, 63

Ouyed, R., Leahy, D., Ouyed, A., & Jaikumar, P. 2011a, Phys. Rev. Lett., 107, 151103

Ouyed, R., Leahy, D., Staff, J., & Niebergal, B. 2009, Adv. Astron., 463521

Ouyed, R., Staff, J., & Jaikumar, P. 2011b, ApJ, 729, 60

Pan, T., Loeb, A., & Kasen, D. 2012, MNRAS, 2979

Pastorello, A., et al. 2010, ApJL, 724, L16

Quimby, R., Castro, F., Mondol, P., Caldwell, J., & Terrazas, E. 2007a, Central Bureau Electronic Telegrams, 793, 1

Quimby, R. M., Aldering, G., Wheeler, J. C., Höflich, P., Akerlof, C. W., & Rykoff, E. S. 2007b, ApJ, 668, L99

Quimby, R. M., Castro, F., Gerardy, C. L., Hoeflich, P., Kannappan, S. J., Mondol, P., Sellers, M., & Wheeler, J. C. 2005, BAAS, 37, 1431

Quimby, R. M., et al. 2011, Nature, 474, 487

Rau, A., et al. 2009, PASP, 121, 1334

Smith, N., Chornock, R., Li, W., Ganeshalingam, M., Silverman, J. M., Foley, R. J., Filippenko, A. V., & Barth, A. J. 2008, ApJ, 686, 467

Smith, N., Chornock, R., Silverman, J. M., Filippenko, A. V., & Foley, R. J. 2010, ApJ, 709, 856

Smith, N., et al. 2007, ApJ, 666, 1116

Smith, N., & McCray, R. 2007, ApJ, 671, L17

Staff, J. E., Ouyed, R., & Jaikumar, P. 2006, ApJL, 645, L145

Vogt, C., Rapp, R., & Ouyed, R. 2004, Nuclear Phys. A, 735, 543

Weidemann, V. 1977, A&A, 59, 411

Wenger, S., Ament, M., Steffen, W., Koning, N., Weiskopf, D., & Magnor, M. 2012, Computing in Science and Engineering, 14, 78

Witten, E. 1984, Phys. Rev. D, 30, 272

Woosley, S. E. 2010, ApJ, 719, L204

Woosley, S. E., Blinnikov, S., & Heger, A. 2007, Nature, 450, 390

Xu, R. X., Zhang, B., & Qiao, G. J. 2001, Astroparticle Phys., 15, 101

Young, D. R., et al. 2010, A&A, 512, A70

Yungelson, L. R., van den Heuvel, E. P. J., Vink, J. S., Portegies Zwart, S. F., & de Koter, A. 2008, A&A, 477, 223

N. Koning, M. Kostka, D. Leahy, and R. Ouyed: Department of Physics and Astronomy, University of Calgary, Calgary, AB, Canada, T2N 1N4 (nico.koning, mkostka, leahy, rouyed@ucalgary.ca).

W. Steffen: Instituto de Astronomía Universidad Nacional Autónoma de México, Ensenada, B.C., Mexico (wsteffen@astro.unam.mx).